NUMERICAL INVESTIGATION OF CONJUGATE HEAT TRANSFER IN A HEAT EXCHANGER EQUIPPED WITH CROSS-COMBINED ELLIPSOIDAL DIMPLE TUBES

Changquan Hu[1], Xiaobo Feng[1], Zeng Yuan[1,2], Dajun Shen[1], Liang Zhang[*3], Jiyu Zheng[3]

1. Chongqing Gas Field of Petro China Southwest Oil and Gas Field Company, Chongqing 400707, PR China

2. College of Materials Science and Engineering, Chongqing University, Chongqing 400044, PR China

3. School of Mechatronic Engineering, Southwest Petroleum University, Chengdu, Sichuan 610500, PR China

Corresponding author: Liang Zhang, School of Mechatronic Engineering, Southwest Petroleum University, Chengdu, Sichuan 610500, PR China. Tel.:+862883035678,

E-mail: dc_zhang2022@163.com

Abstract*: At present, most numerical methods consider the tube walls as the same constant temperature in the simulations of the heat exchanger, and only the external fluid outside the tubes is considered. To investigate the heat transfer performance of the heat exchanger in the real running state, a conjugate heat transfer simulation is performed for a heat exchanger equipped with cross-combined ellipsoidal dimple tubes in this paper. The k-ε standard turbulence model is selected to simulate the heating process of tube bank. The distributions of the temperature field and flow field are analyzed carefully. The results indicate that the temperature distribution and the heat flux on the tube wall are uneven, which is different from the case regarding the wall boundaries as a constant temperature. The heat transfer performance of the dimpled tube is higher than that of the smooth tube in the heat exchanger, and the heat transfer performance for aligned arrangement is better than that for staggered arrangement. In addition, the influences of geometric and flowing parameters on heat transfer are discussed.*

Keywords*: Conjugate heat transfer; Heat exchanger; Cross-combined ellipsoidal dimple tube; Heat transfer performance*

1. Introduction

In many industrial applications, the fluid flows over some tube surfaces so as to exchange the heat between the internal fluid and external fluid. In most cases, the direction of the two fluids is orthogonal, which leads to the development of cross-flow heat exchangers. Cross-flow heat exchangers are widely used in many

industrial applications, such as petrochemical industries, Heating Ventilation Air Conditioning (HVAC) systems, and aerospace fields. To improve the heat transfer efficiency, various measures of the heat transfer enhancement have been proposed for the heat exchanger. The heat transfer enhanced tube in the shell-and-tube heat exchangers has increasingly attracted much attention in the heat transfer enhancement techniques.

Roughening the tube surface is commonly applied in heat exchanger because of its low-pressure drop [1]. The heat transfer enhancement technologies utilizing dimples surfaces have become the focus of research in recent years [2]. An enhanced surface disturbs the flow inside the tube, leading to greater turbulence intensity and disruption of the boundary layer [3, 4].

Many researchers have been focused on the flow and heat transfer characteristics inside or outside a single heat transfer enhanced tube, especially the tubes with various shapes dimples [5,6]. An experiment investigated the complicated flow patterns in the channel with cylindrical and spherical dimples [3]. The result showed that when ***Re*** (Reynolds number) is higher than 10000, the cylindrical dimple has the most extended separation band. Wang et al. [7] investigated the heat transfer of the tube with ellipsoidal dimples and spherical dimples. Compared with the smooth tube, the Nusselt numbers increase by 38.6–175.1% and 34.1–158% respectively, while the friction factors increase by 26.9–75% and 32.9–92% respectively. Wang et al. [8] studied the hydraulic and heat transfer characteristics of dimpled tubes with different arrangements. The corresponding results showed that effects on the flow and heat transfer performances differ from the arrangement within 5%. The numerical results showed that the heat transfer enhancement is induced owing to the centrally located vortex pairs appearing near the spanwise edges of individual dimples [9,11]. CFD (Computational Fluid Dynamics) simulations were carried out to study the effects of geometric parameters on the overall performance. Investigation of an enhanced tube using experimental and numerical simulation techniques was presented to depict the thermal-hydraulic performance, and the relative error between the experimental result and the numerical result is within 10% [11]. In addition, the local details from the simulation revealed that dimples could disturb the boundary layers and generate secondary flows, which improves turbulence levels.

For the cross-flow heat exchangers, previous studies primarily focus on the cross-flow heat exchanger equipped with the smooth circle tube. With the development of research and application of enhanced heat transfer technology, the cross-flow heat exchanger equipped with the heat transfer enhanced tube has been studied a lot [12,13]. Experimental and numerical investigations by Matos et al. [14] indicated that the elliptic tubes performed better heat transfer performance than circular ones. Lavasani et al. [15,16] carried out the experimental and numerical investigations on the cam-shaped tube bundles to conclude that the heat transfer performance of cam-shaped tube bundles performs better than that of circular tube bundles. Alawadhi [17] explored the effect of progressive attack angle on the laminar forced convection for the in-line elliptical cylinder tube, and the progressive inclination varied from 0° to 90°. Besides, further research in the more streamlined tubes continues, such as the lenticular and elliptical cylinders [18,19] The heat transfer numerical simulation of exchangers with elliptical tubes was carried out to investigate tube pitch influence [20]. The results show that the overall heat transfer efficiency of the tube bank with elliptical tubes is higher than that with smooth tubes, and the total heat transfer efficiency and pressure drop increase with the increase of transverse tube spacing. Kong et al. [21] investigated the heat transfer performance of the heat exchanger with flat-fin and slit-fin numerically and described the heat transfer performance in a correlation.

The experimental and the 3D numerical simulation of cross flow tube bundle in staggered arrangements with the splitter plate attachment is performed [22]. The results showed that the provision of the splitter plate

can improve the heat transfer performance and decrease the pressure drop. An increase of 60 - 82% in the overall thermal performance was observed at *Re* = 5500.

In previous studies, the thermal–hydraulic characteristics inside or outside the heat transfer enhanced tube have been considered separately. At the same time, the tube walls of the fluid domain were simplified as constant temperature or constant heat flux, which does not take into consideration the thermal interactions between the internal flow and external flow caused by the existing recirculation zones. To reveal the realistic reproduction of the coupled heat transfer among the external flow, the tubes with dimples, and the internal flow, CFD numerical simulations were performed based on the cross-combined ellipsoidal dimple tube (The numerical investigation has been carried out, and the result showed that the cross-combined ellipsoidal dimple tube performs superior performance in heat transfer [3].) in the heat exchanger. The thermal performance of the heat exchanger is revealed by the temperature rise and the distribution of temperature and heat flux. Moreover, various parameters such as transverse pitch, longitudinal pitch, Reynolds number, and heated section length are investigated. The results in this paper provided better practical guidelines in industrial applications.

2. Mathematical model and numerical method

2.1. Geometry model

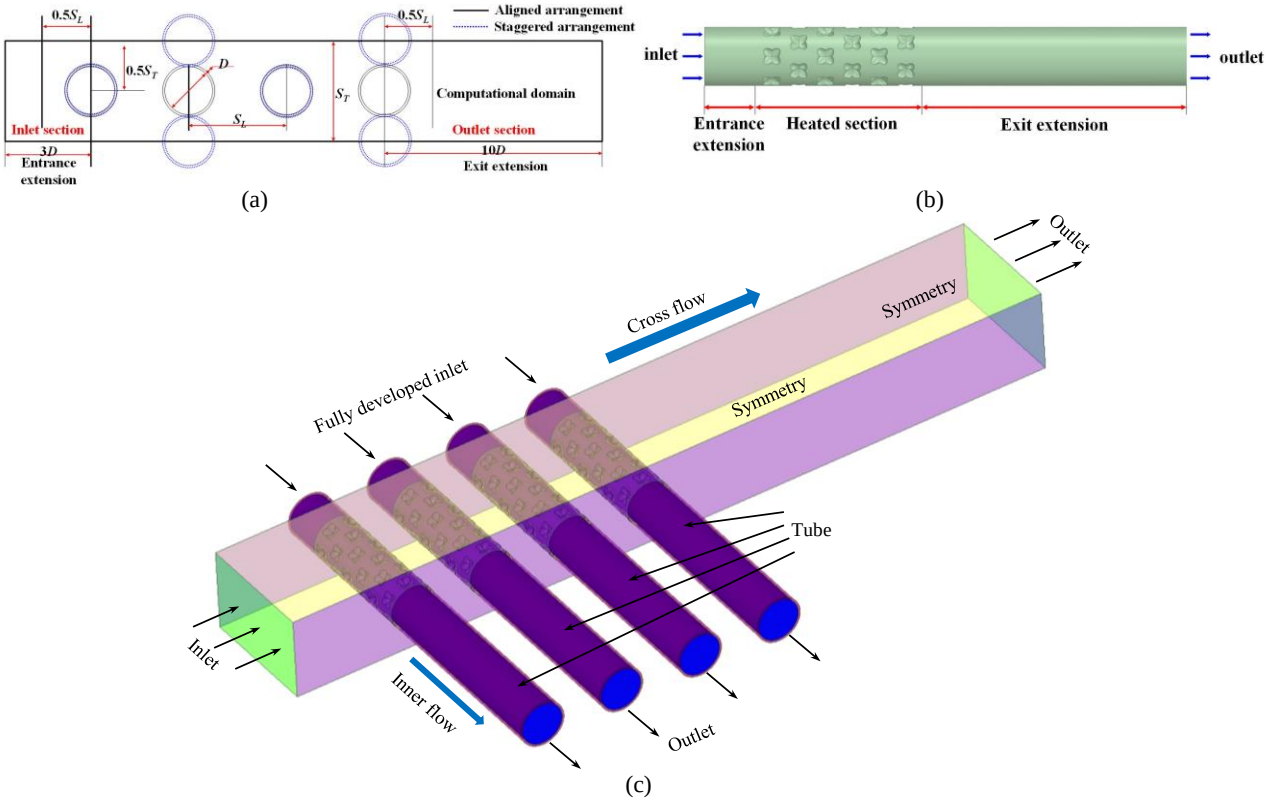

Figure 1. Schematic diagram of the heat exchanger: (a) Cross-combined ellipsoidal dimple tube; (b) Arrangement parameters of the tube bank; (c) Overall computational domain of the heat exchanger (Aligned arrangement).

Fig. 1 shows the schematic diagram of the heat exchanger equipped with cross-combined ellipsoidal dimple tubes. The overall geometry model consists of three parts: cross-combined ellipsoidal dimple tube

region, internal flow region, and cross flow region. The fluid inside the tubes is cold fluid, and the fluid outside the tubes is hot fluid.

The cross-combined ellipsoidal dimple tube is shown in fig. 1(a), two ellipsoidal dimples are interlaced to form a cross-combined dimple, all of which are equidistantly arranged in the axial direction on the surface (Geometric parameters is detailed in reference [23]). The inner diameter of the tube is 20 mm and the outer diameter is 22 mm. The length of the heated section L_H is 60 mm. A distance of 20 mm is extended from the heated section to the inlet section, and a distance of 90 mm is extended from the heated section to the outlet section to prevent the influence of backflow on the test region.

Fig. 1(b) shows the arrangement parameters of the tube bank for cross flow. Both transverse pitch S_L and longitudinal pitch S_T are 40 mm. At the same time, to eliminate the influence of the inlet end and backflow on computational domain, the lengths of inlet section and outlet section are increased by three times and ten times of the tube diameter respectively. Fig. 1(c) shows the global computational domain of the heat exchanger with cross-combined ellipsoidal dimple tubes.

2.2. Governing equations

Simulations on forced convection for the heat exchanger equipped with cross-combined ellipsoidal dimple tubes are performed based on the commercial CFD code Fluent. The solution of the fluid flow analysis is based on the governing equations [24,25]. The mass, momentum, and energy conservative equations for the steady flow can be written as:

Mass conservative equation:

$$\frac{\partial}{\partial x_i}(\rho u_i) = 0 \tag{1}$$

Momentum conservation equation:

$$\frac{\partial}{\partial x_j}(\rho u_i u_j) = -\frac{\partial p}{\partial x_i} + \frac{\partial}{\partial x_j}\left(\mu + \mu_t\right)\left(\frac{\partial u_i}{\partial x_j} + \frac{\partial u_j}{\partial x_i}\right) \tag{2}$$

Energy conservative equation:

$$\frac{\partial}{\partial x_i}(u_i T) = \frac{\partial}{\partial x_i}\left[\left(\frac{\mu}{Pr} + \frac{\mu_t}{Pr_t}\right)\frac{\partial T}{\partial x_i}\right] \tag{3}$$

where $\boldsymbol{\rho}$ is the fluid density, $\boldsymbol{u}$ is the velocity vector, $\boldsymbol{p}$ is the pressure, $\boldsymbol{\mu}$ is the dynamic viscosity, $\boldsymbol{c_p}$ is the specific heat, $\boldsymbol{T}$ is the temperature, $\boldsymbol{Pr}$ is the Prandtl number.

The heat transfer mode is heat conduction in solid region. The heat conduction equation is described as follows.

$$\rho c_p = \nabla\cdot(\lambda \nabla T) \tag{4}$$

where $\boldsymbol{\lambda}$ is the heat conductivity coefficient.

The realizable k-ε model is adopted in this paper. Equations for turbulence kinetic energy k and specific dissipation rate ε are defined as follows:

$$\frac{\partial}{\partial x_i}\left(\rho u_i k\right) = \frac{\partial}{\partial x_j}\left[\left(\mu + \frac{\mu_t}{\sigma_k}\right)\frac{\partial k}{\partial x_j}\right] + G_k - \rho\varepsilon \tag{5}$$

$$\frac{\partial}{\partial x_i}\left(\rho\varepsilon u_i\right)=\frac{\partial}{\partial x_j}\left[\left(\mu+\frac{\mu_t}{\sigma_\varepsilon}\right)\frac{\partial\varepsilon}{\partial x_j}\right]+C_{1\varepsilon}\frac{\varepsilon}{k}G_k-C_{2\varepsilon}\rho\frac{\varepsilon^2}{k} \tag{6}$$

where k represents the turbulent kinetic energy, ε represents the turbulence dissipation rate, Gk represents the turbulence kinetic energy generated by mean velocity gradient, $C_1\varepsilon$, $C_2\varepsilon$ are constants needed for the turbulent model. The k-ε realizable turbulent model provides excellent performance for simulating the realistic turbulent flow, especially for flows involving rotation, separation and recirculation. The following parameters are employed to characterize heat transfer and flow performances.

Reynolds number predicts the flow pattern in various flow situations, Re is denoted as follows:

$$Re=\frac{\rho v_m D_c}{\mu} \tag{7}$$

where v_m represents the average velocity of the fluid, D_c represents hydraulic diameter. In addition, the Reynolds number inside the tube and the Reynolds number outside the tube are represented Re_{in} and Re_{out}.

Temperature rise means temperature difference between back end and front end of the heated section of the fluid inside the tube. Temperature rise indicates the heat transfer efficiency of the heat exchange tube more visually. ΔT_d are defined as:

$$\Delta T_d = T_{inner,back} - T_{inner,front} \tag{8}$$

Where $\boldsymbol{T}_{\boldsymbol{inner,\ back}}$ represents the temperature at the inlet of the inner flow, $\boldsymbol{T}_{\boldsymbol{inner,\ front}}$ represents the temperature at the outlet of the inner flow.

For the current study, the governing equations are solved by the ANSYS Fluent software. The simulations are converged when the residual curve of all equations is less than 10^{-6} and the wall heat flux as well as wall temperature reach stable. The pressure and velocity fields are coupled by the Coupled algorithm. The discrete format of the pressure correction equation uses the second order, and the second-order upwind style is adopted in the discrete equations for the momentum, turbulent energy, dissipation rate and energy equations.

2.3. Boundary conditions

For the inner flow, the velocity inlet with a fully developed flow is set at the tube inlet with a backflow turbulence intensity of 5% and backflow turbulence viscosity ratio of 10. The outlet boundary condition is selected as pressure-outlet, and the backflow temperature is set as 300 K. For the external flow, the setting of inlet and outlet is the same as the inner flow. The velocity of internal fluid and external fluid are 9 m/s and 3 m/s respectively. Because the temperature rise is small, the thermophysical properties are regarded as constant.

Cross-combined ellipsoidal dimple tubes are made of copper with good thermal conductivity to enhance heat transfer performance. Air is selected as the work medium. The temperature at the inlet is defined as 300 K for internal flow and 400 K for external flow, resulting in the heat transfer from external flow to internal flow. The tubes are distributed symmetrically in the exchanger, so the upper and lower surfaces of the computational domain are symmetric boundary. Moreover, only the heat exchange of the heated section is concerned. Thermal coupling between the fluid region and the solid region is implemented utilizing contact interfaces, and all the uncoupled walls are considered adiabatic. Besides, the pressure drop and heat transfer enhancement of cross-combined ellipsoidal dimple tubes have been investigated in reference [23].

2.4. Grid independence analysis and model validation

Mesh generation of the computation domain is shown in fig. 2. Four grid numbers are employed to analyze the grid independence. Tab. 1 shows the grid independent analysis for the aligned arrangement and staggered arrangement of the heat exchanger. For aligned arrangement, the variation of ΔT_d is 0.86% when the grid of 1502319 elements increases to that of 2731512 elements, and that is 0.35% with the rise of grid number from 2731512 to 5215176. Thus, the grid of 2731512 elements is selected. Similarly, the grid of 1371856 elements is selected for staggered arrangement.

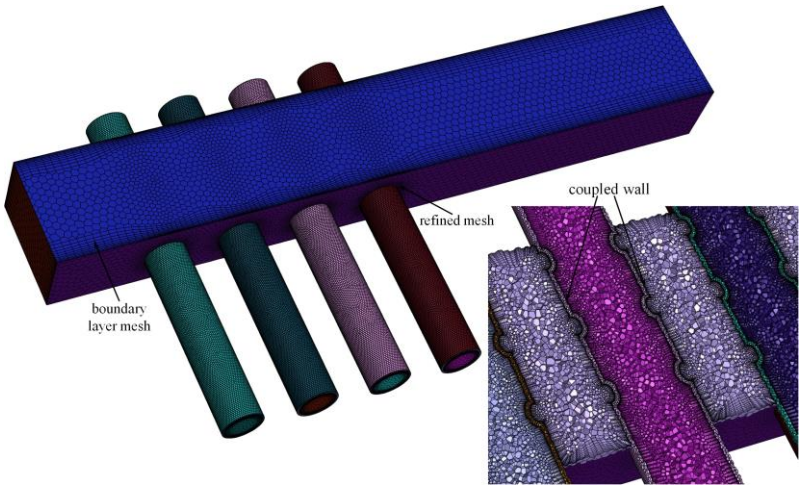

Figure 2. **Mesh generation of the computational domain (Aligned arrangement).**

Table 1. Grid independent test for aligned arrangement and staggered arrangement.

Arrangement	Aligned arrangement			Staggered arrangement		
Mesh	Grid number	ΔT_d (K)	Deviation (%)	Grid number	ΔT_d(K)	Deviation (%)
Mesh1	1035143	5.629	--	603213	6.740	--
Mesh2	1502319	5.714	1.51	864458	6.825	1.26
Mesh3	2731512	5.763	0.86	1371856	6.877	0.76
Mesh4	5215176	5.783	0.35	2815317	6.906	0.42

In order to validate the numerical model of turbulent flow, the numerical results were compared to the empirical results. As shown in fig. 3(a), the numerical results were compared to Gnielinski correction [26] for *Nu* (Nusselt number) and Petukhov correction for *f*.

$$Nu = \frac{hD_h}{\lambda} \qquad f = \frac{2\Delta p}{\rho u_i^2}\frac{D_h}{L} \tag{9}$$

Where h is the convection heat transfer coefficient, D_h is the equivalent diameter, Δp is the pressure drop of the test section, and L is the length of the test section.

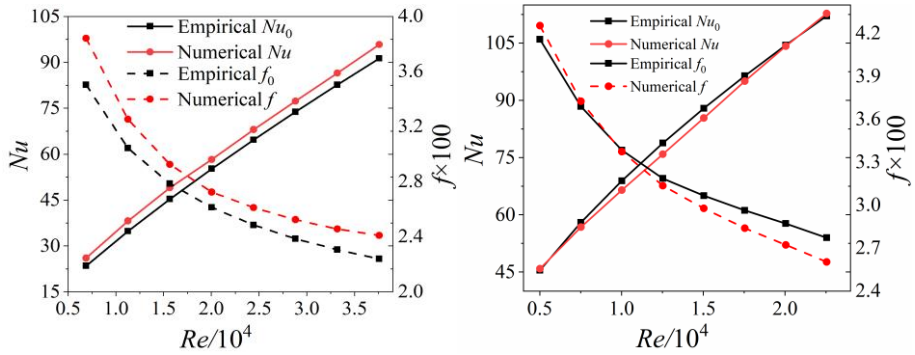

(a)Internal fluid (b) External fluid

Figure 3. Validation of numerical model: (a)Internal fluid (b)External fluid

It was found that the deviations of smooth tube are within 15%. Similarly, the numerical results for external fluid in the tube bank were compared to empirical correction [27], as shown in fig. 3(b). It can be seen that the deviations of tube bank are within 10%, which indicates that the numerical model agreed with the empirical corrections.

3. Result and discussion

3.1. Heat transfer characteristic of heat exchanger

3.1.1 Heat transfer and flow characteristic

Fig. 4 shows the distribution of streamlines, velocity, and temperature of the external fluid for aligned arrangement. An area with low velocity is formed in front of the tube in the first row because the windward side of the tube is shocked by the flow. And then, the fluid is separated into two parts by every tube. In addition, it can be seen that the velocity is higher above and below the tube, while the velocity behind the dimpled tube is lower. The flow velocity increases when the fluid passes through the tube bank because the flow cross-section shrinks. A pair of vortex forms behind every tube, and the size and position of the vortices are not symmetrical; this is because the tubes in the latter row carry out a blocking effect to the wake generated by the tube in the preceding row. In the external fluid zone, the region with lower temperature appears in the region with the lower flow velocity. The fluid has a longer residence time in the low-velocity region, resulting in an adequate heat transfer between the fluid and the tube walls.

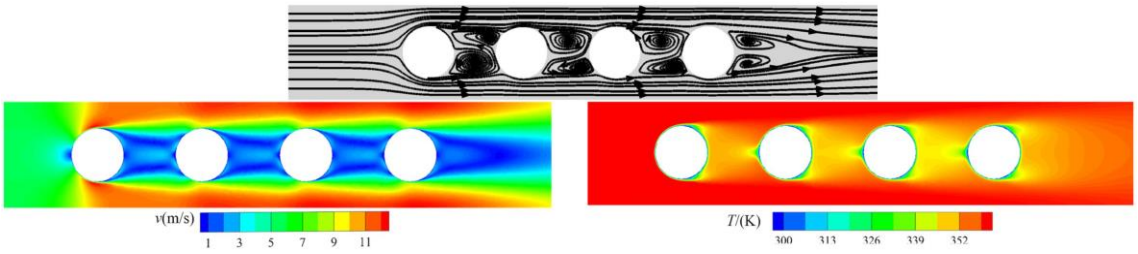

Figure 4. Streamlines, velocity, and temperature distribution of the external fluid for aligned arrangement

Fig. 5 shows the distribution of temperature and heat flux of the tube walls for aligned arrangement. One finds that the temperature distribution and heat flux of the tube walls is not uniform.

The hot external fluid flows across the low-temperature tube, and the heat is transferred into the tube. The average temperature of the tube wall from the first row to the fourth row along the flow direction is 329.42 K, 327.16 K, 325.73 K, and 326.05 K, respectively. The average temperature change from the first row to the third row is very drastic, while the change from the third row to the fourth row is very slight. In particular, the average temperature of the fourth row is higher than that of the third row. In the first three rows, the backflows are generated between the two tubes. The fluid makes sufficient contact with the front and rear tubes. However, the tube of the fourth row is not affected by the rear tube, so that the average temperature of the fourth row rises marginally. For the single tube, the temperature in the middle of the heated section is higher than that at both ends, and the temperature downstream is marginally higher than that upstream. In addition, the temperature on the windward side is higher than that on the leeward side, as shown in fig. 5(c) left side. The hot external fluid flows straight to the windward side of the tube, but the velocity in the leeward side is low because of the backflow, leading to a sufficient contact between the hot external fluid and cold tube walls.

The change of average heat flux is similar to that of the temperature. The average heat flux of the tube walls from the first row to the fourth row along the flow direction are 3877 W/m^2, 3579 W/m^2, 3390 W/m^2, and 3437 W/m^2, respectively. The heat flux inside the dimples is lower than that outside the dimples.

For the single tube in the first row, the maximum local value appears at θ=0° (Forward stagnation-point), and θ = 180° (Backward stagnation-point), and the local heat flux on the windward side is higher than that on the leeward side. At θ = 0°, the temperature gradient has the maximum value, and the heat transfer driving force has the maximum value. Moreover, the local maximum heat flux appears at θ=180° because of the attached vortex in the rear of the tube. However, the local heat flux reduces gradually around the tube in that the heat boundary layer becomes thick gradually. When θ = 120°, the local minimum heat flux appears because of the flow separation.

For the tubes in the latter few rows, the maximum local value appears at θ = 60° and θ = 180°, and the local minimum value appears at θ = 0° and θ = 120°(see fig. 5(c) left side). The tubes in the latter few rows are affected by the wake generated by the first row so that the stagnation-point moves from θ = 0° to θ = 60°. The local heat flux has little change at θ = 180°, indicating that the position of backward stagnation-point remains essentially the same as that of the first row.

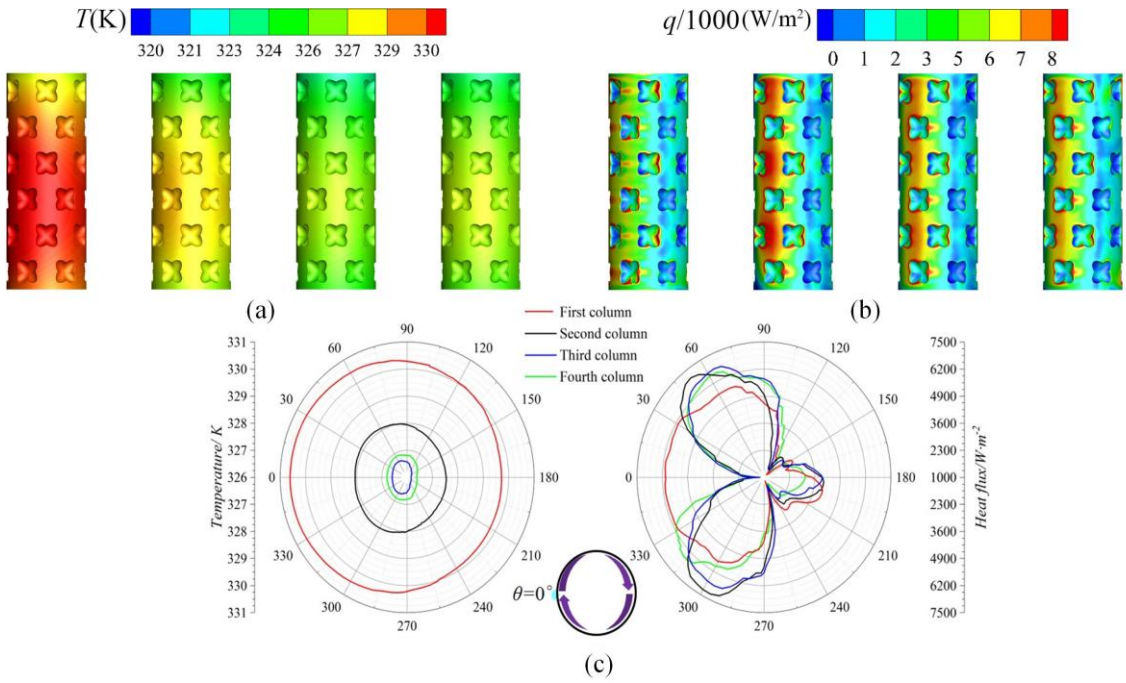

Figure 5. Distribution of wall temperature (a), heat flux (b), and local temperature and heat flux around the tube(c) for aligned arrangement.

Fig. 6 shows the distribution of streamlines, velocity, and temperature of the external fluid for staggered arrangement. Similarly, when the external fluid flows across the tube bank, the flow velocity changes alternately because of the reduction and expansion of the flow cross-section. Compared to the aligned arrangement, the development of the backflow is not full, and the distribution of the streamlines is compact. This is because the pressure of the backflow region is higher for staggered arrangement, inhibiting the development of the backflow and vortex. In addition, the distribution of temperature for staggered arrangement is more uneven comparing with it for aligned arrangement. The direction of the adjacent tubes is the same as the flow direction for aligned arrangement so that it is less disturbed. However, the external fluid is disturbed strongly for staggered arrangement, which leads to a relatively drastic temperature change.

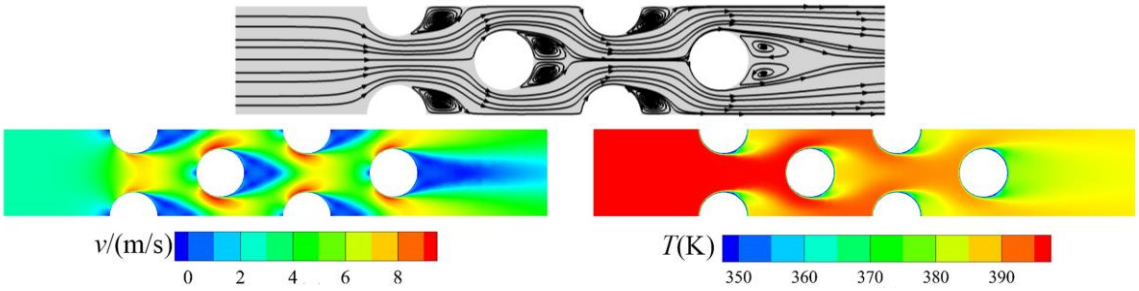

Figure 6. Streamlines, velocity and temperature distribution of the external fluid for staggered arrangement.

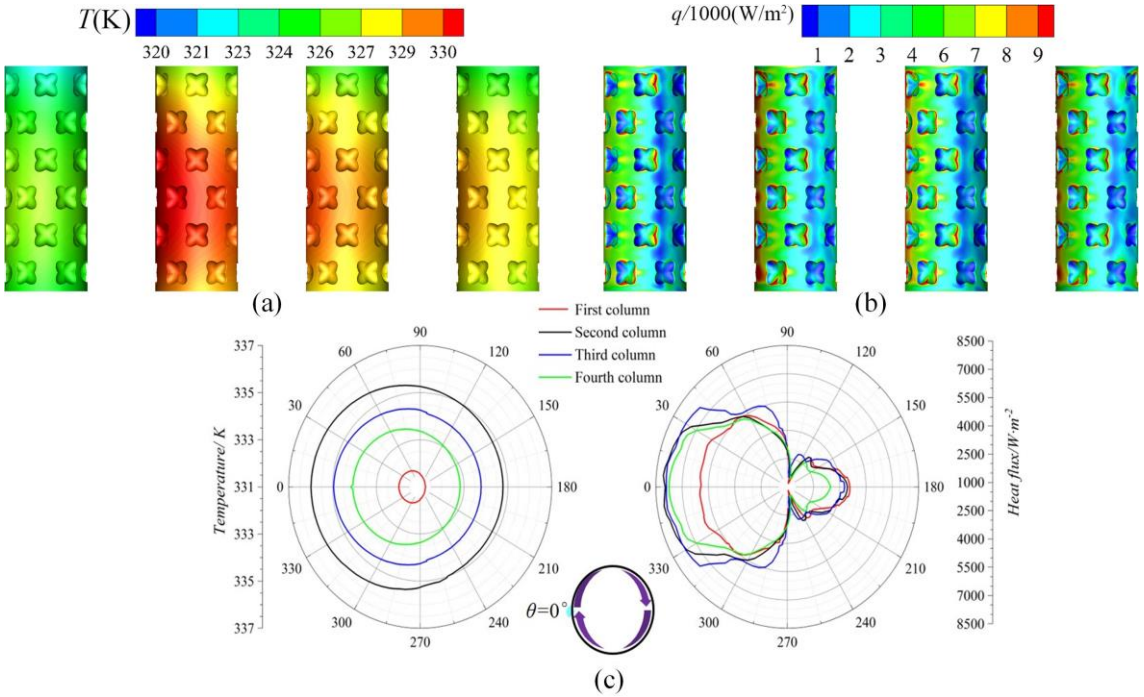

Figure 7. Distribution of wall temperature (a), heat flux (b), and local temperature and heat flux around the tube (c) for staggered arrangement.

Fig. 7 shows the distribution of temperature and heat flux of the tube walls for staggered arrangement. It can be seen that the distribution of temperature and heat flux of the tube walls for staggered arrangement is different from that for the aligned arrangement. The average temperature of the tube walls from the first row to the fourth row is 330.34 K, 334.00 K, 333.00 K, and 332.15 K, respectively. According to the simulation results, the average temperature of the first row is the lowest, which is different from that for aligned arrangement. The flow cross-section in front of the second row shrinks, the external hot fluid scours the tube of second row at a high speed. Thus, the highest average temperature appears in the second row. After the first row, the average temperature decreases along the flow direction in that the external hot fluid is cooled gradually. Moreover, the maximum temperature difference of the average temperature for the staggered arrangement is higher than that of the aligned arrangement. For the single tube, the wall temperature distribution is similar to that for aligned arrangement (see fig. 7(c) left side).

The heat flux change is similar to that of temperature (see fig.7 (b)). The average heat flux of the tube wall from the first row to the fourth row along the flow direction is 4015 W/m^2, 4497 W/m^2, 4363 W/m^2, and 4259 W/m^2, respectively. For the single tube, the local heat flux distribution is similar among the different rows(see fig. 7(c) right side). Among these, the local heat flux of the windward side in the first row is lower than the others. The flow cross-section in front of the first row is greater than the others, and the degree to which the external fluid scours on the tube wall is not intense.

According to the simulation results of aligned and staggered arrangements, we can find that the distribution of temperature and heat flux of the tube walls is uneven, and the distribution of temperature and heat flux for both arrangements is different. The flow characteristic of the external fluid leads to an uneven distribution of temperature and heat flux. Thus, constant thermal boundary conditions are not reasonable in the simulation of the heat exchanger.

3.1.2 Evaluation of heat transfer performance

According to the previous study in this paper, we have found that the distribution of wall temperature and heat flux is uneven. Thus, the actual heat transfer in the exchanger is different from which regarding the walls as constant temperature walls. Fig. 8 shows the outlet temperature of the heated section for aligned and staggered arrangements. It can be seen that the high-temperature area is concentrated near the wall, and the near-wall temperature for staggered arrangement is higher than that for aligned arrangement, indicating that it has a better heating efficiency for staggered arrangement. At the same time, the high-temperature area for staggered arrangement is more significant than that for aligned arrangement.

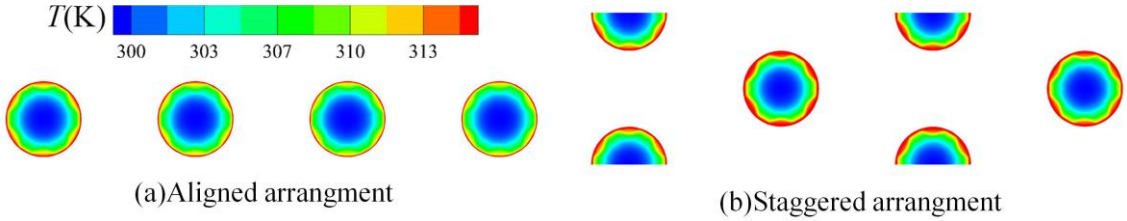

Figure 8. Outlet temperature of the heated section: (a)aligned arrangement, (b)staggered arrangement

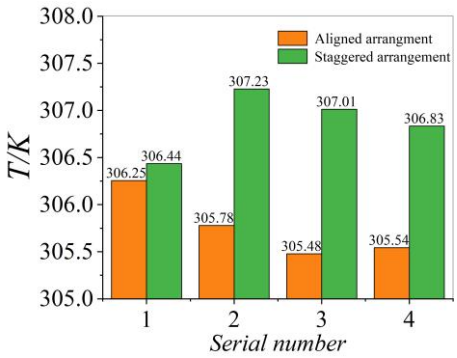

Figure 9. Average outlet temperature of the heated section at different tube locations

Fig. 9 shows the average outlet temperature of the heated section for the two arrangements. It can be found that the distribution of the average outlet temperature is similar to that of the wall temperature and heat flux. The outlet temperature for aligned arrangement is higher than that for staggered arrangement in all the tubes. For aligned arrangement, the average temperature gradually drops from the first row to the third row and increases at the fourth row marginally, with the maximum temperature difference of 0.78 K. For staggered arrangement, the average temperature of the first row is the lowest, and that of the second row is the highest. The maximum temperature difference is 0.79 K. From the second row to the fourth row, the average temperature
gradually drops. In conclusion, the results indicate that the boundary conditions of the tube wall can affect the heating degree of the internal fluid, resulting in different outlet temperatures.

3.1.3 Comparison of heat transfer performance

To indicate that the cross-combined ellipsoidal dimple tube has a good effect of heat transfer enhancement in the application of the heat exchanger, the temperature rise of the heated section of the cross-combined ellipsoidal dimple tube is compared with that of the smooth tube under the same boundary

conditions, as shown in fig. 10.

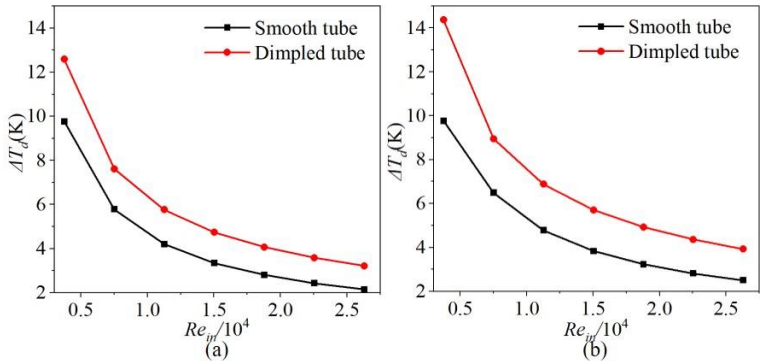

Figure 10. Temperature rise of dimpled tube and smooth tube in the heat exchanger for aligned arrangement (a) and staggered arrangement (b).

As can be seen, the temperature rise decreases with the increase of Re_{in}, and the rate of decline of temperature rise gradually decreases. This is because the residence time of the fluid is shorter for high-speed flows, resulting in less heat exchanged with the wall. More importantly, the temperature rise of the cross-combined ellipsoidal dimple tube is higher than that of the smooth tube, and the temperature rise of the staggered arrangement is higher than that of the aligned arrangement. For the aligned arrangement, the temperature rise of the cross-combined ellipsoidal dimple tube is 3.21 -12.58 K, and that of the smooth tube is 2.15 - 9.76 K. Compared with the smooth tube, the temperature rise of the cross-combined ellipsoidal dimple tube improves 28.85% - 49.37%. Likewise, for the staggered arrangement, the temperature rise of the cross-combined ellipsoidal dimple tube is 3.92 -14.36 K, and that of the smooth tube is 2.50 - 9.76 K. Compared with the smooth tube, the temperature rise of the cross-combined ellipsoidal dimple tube improves 37.82% - 56.63%.

Compared with the smooth tube, the results show that cross-combined ellipsoidal dimple tube conduces to the heat transfer enhancement. In addition, the arrangement of the tube bank has little influence on the temperature rise of the smooth tube but a significant influence on the temperature rise of the dimple tube.

3.2. Influence of parameters on heat transfer performance

3.2.1 Transverse pitch and longitudinal pitch

The effects of pitch, Re_{out}, and heated section length are studied under the same simulation conditions. The variations of ΔT_d under different longitudinal pitches and transverse pitches are revealed in fig. 11 and fig. 12.

It is found that the change of temperature rise is tiny under different longitudinal pitches, indicating that longitudinal pitch has little influence on temperature rise. However, the effect of the transverse pitch on temperature rise is obvious. The temperature rises decreases with the increase of the transverse pitch, and the extent of temperature rises change is gradually stable with the increase of Re_{in}. Thus, the influence of transverse pitch on the heat transfer effect should be considered firstly in the actual production.

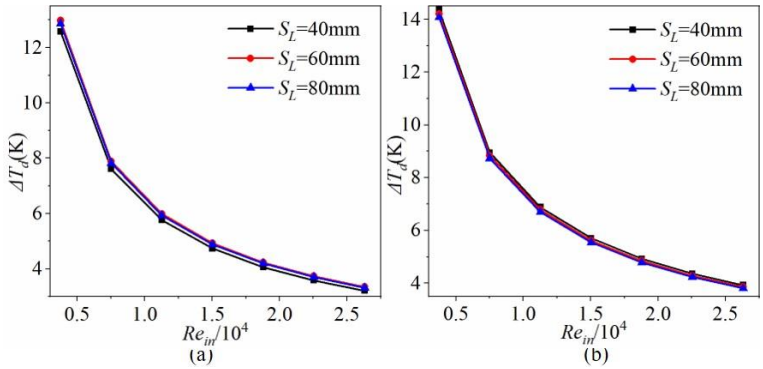

Figure 11. Effect of longitudinal pitch S_L on the temperature rise for aligned arrangement (a) and staggered arrangement (b).

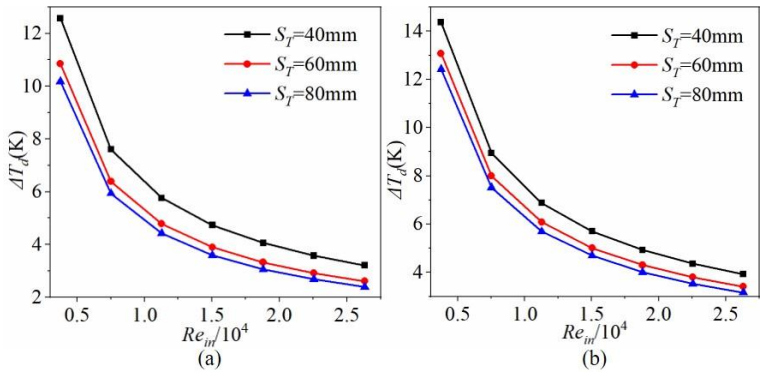

Figure 12. Effect of transverse pitch S_T on the temperature rise for aligned arrangement(a) and staggered arrangement(b).

3.2.2 Reynolds number of the external flow

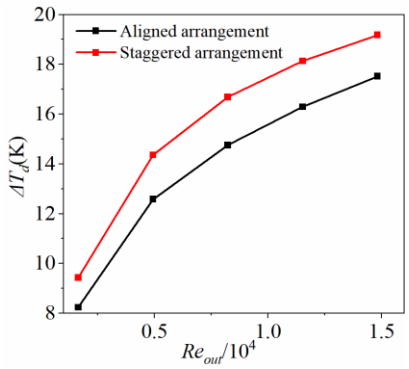

Figure 13. Distribution of the temperature rise under different Re_{out}

It can be seen from the previous contents that the flow characteristics of the external fluid have a significant influence on the heat transfer performance. Fig. 13 shows the ΔT_d for aligned arrangement and staggered arrangement under different Re_{out}. It is revealed that the ΔT_d increases with the increase of Re_{out}, this is because that the external flow scours tube walls more drastically, and more heat is transferred into the tube. In addition, the ΔT_d for staggered arrangement is more significant than that for aligned arrangement, indicating it has a better heat transfer performance for staggered arrangement. Furthermore, the rate of ΔT_d

rises becomes slow gradually with the increase of Re_{out}.

3.2.3 Heated section length

Fig. 14 shows the changing trend of ΔT_d under different heated section lengths. It can be seen that the influence of changing trend of ΔT_d is similar for aligned arrangement and staggered arrangement. ΔT_d increases with the increase of the heated section length, but the degree of increase decreases gradually. As the heated section length increases, the temperature of the internal fluid increases, and the temperature of the external fluid drops. As a result, when the heated section length reaches a critical value, the temperature difference between the internal fluid and the external fluid is 0, reaching an equilibrium state eventually. In addition, for the two arrangements, the degree of ΔT_d growth at the low Re_{in} is higher than that at the high Re_{in} with the increase of the heated section length. This is because that the rise of Re_{in} makes the effect of destroying the boundary layer more apparent, especially at the low Re_{in}.

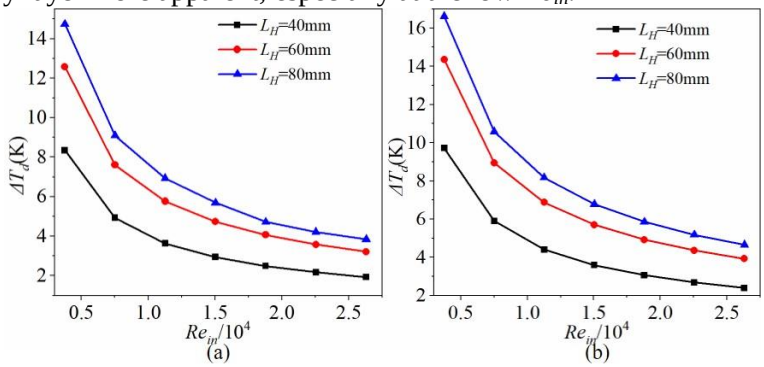

Figure 14. Distribution of the temperature rise under different L_H or aligned arrangement (a) and staggered arrangement (b)

4. Conclusions

In this paper, the conjugate heat transfer simulations are carried out for the heat exchanger equipped with cross-combined ellipsoidal dimple tubes, leading to realistic running status of the coupled heat transfer among the external flow, the internal flow, and the dimpled tubes. In this work, the temperature rise ΔT_d of the heated section is used to evaluate the heat transfer performance, and the distribution of temperature, velocity, and heat flux are presented to show the characteristics of flow and heat transfer. The main conclusions are drawn as follows:

(1) The distribution of wall temperature and heat flux is uneven under actual working conditions. The temperature rise of the heated internal flow varies with different positions, and it is affected by the arrangement mode. For the aligned arrangement, the outlet temperature of internal fluid decreases firstly and then increases. For the staggered arrangement, the outlet temperature of the internal fluid increases firstly and then decreases. The outlet temperature of internal fluid for staggered arrangement is higher than that for aligned arrangement, indicating that the heating effect for staggered arrangement is better than that for aligned arrangement.

(2) Compared the heat transfer performance of the cross-combined ellipsoidal dimple tube with smooth tube in the heat exchanger, it is found that the temperature rise of the cross-combined ellipsoidal dimple tube is significantly higher than that of the smooth tube, and the maximum increasing extents of the temperature rise are 49.37% and 56.63% for aligned arrangement and staggered arrangement, respectively.

(3) The influence of the different geometric and flowing factors on the heat transfer performance for the heat exchanger is investigated. The heat transfer performance of the heat exchanger is mainly affected by the tube pitch, *Re* of the external flow, and the heated section length. ΔT_d decreases with the increase of the transverse pitch S_T and increases with the increase of Re_{out} and the heated section length. However, ΔT_d changes little with the variation of the longitudinal pitch S_L.

Acknowledgment

This research is supported by Chongqing Gas Field of Petro China Southwest Oil and Gas Field Company.

References

[1] Kim, J., and Choi, H., Aerodynamics of a golf ball with grooves, *P I. Mech. Eng. P-J. Spo*, *228*(2014), 4, pp. 233-241, DOI No. 10.1177/175433114543860.

[2] Ceren H, Gulsah C., Heat transfer analysis of double tube heat exchanger with wavy inner tube, *Thermal Science*, *26*(2022), 4, pp:3455-3462, DOI NO. 10.2298/TSCI210628266H.

[3] Mahmood, Gazi I., *et al*., Local heat transfer and flow structure on and above a dimpled surface in a channel, *Trans. ASME, J. Turbomach*, *123*(2001), 1, pp. 115-123, DOI No.10.1115/1.1333694.

[4] Xie, G., *et al*., Numerical analysis of flow structure and heat transfer characteristics in square channels with different internal-protruded dimple geometrics, *Int. J. Heat Mass Trans*, *67*(2013), pp. 81-97.

[5] Kaood, A., *et. al*., Numerical investigation of the thermal-hydraulic characteristics of turbulent flow in conical tubes with dimples, *Case Studies in Thermal Engineering*, *36*(2022), pp.102166.

[6] Sinaga, N., *et al*. Second law efficiency analysis of air injection into inner tube of double tube heat exchanger. *Alexandria Engineering Journal*, *60*(2021), 1, pp. 1465-1476.

[7] Wang, Y., *et al*., Heat transfer and hydrodynamics analysis of a novel dimpled tube, *Exp. Therm. Fluid Sci*, *34*(2010), 8, pp. 1273-1281.

[8] Wang, Y., *et al*., Heat Transfer and Friction Characteristics for Turbulent Flow of Dimpled Tubes, *Chem. Eng. Technol*, *32* (2009), 6, pp. 956-963 .

[9] Park, J., *et al*., Numerical predictions of flow structure above a dimpled surface in a channel, *Numer. Heat Transfer, Part A*, *45*(2004), 1, pp. 1-20, DOI No. 10.1080/1040778049026740.

[10] Won, S.Y., *et al*., Numerical Analysis of Flow Structure Above Dimpled Surfaces with Different Depths in a Channel, Numer. *Heat Transfer, Part A, 67* (2015), 8, pp. 827-838.

[11] Li, M., *et al*., Single phase heat transfer and pressure drop analysis of a dimpled enhanced tube, *Appl. Therm. Eng*, *101*(2016), 1, pp.38-46.

[12] Lee, D., *et al.*, Uneven longitudinal pitch effect on tube bank heat transfer in cross flow. *Appl. Therm. Eng*, *51*(2013), 1-2, pp. 937-947, DOI No. 10.1016/j.applthermaleng.2012.10.031.

[13] Zhao, L. P., *et al.*, Parametric study on rectangular finned elliptical tube heat exchangers with the increase of number of rows, *Int. J. Heat Mass Trans*, *126*(2018), Part A, pp. 871-893.

[14] Ibrahim, T.A., and Gomaa, A., Thermal performance criteria of elliptic tube bundle in crossflow, *Int. J. Heat Mass Transfer*, *48*(2009), 11, pp. 2148-2158, DOI No. 10.1016/j.ijthermalsci.2009.03.011.

[15] Lavasani, A.M., *et al*., Experimental study of convective heat transfer from in-line cam shaped tube bank in crossflow, *Appl. Therm. Eng*, *65*(2014), 1, pp. 85-93.

[16] Bayat, H., *et al.*, Experimental study of thermal–hydraulic performance of cam-shaped tube bundle with staggered arrangement, *Energy Convers. Manage*, *85*(2014), pp. 470-476.

[17] Alawadhi, E.M. Laminar forced convection flow past an in-line elliptical cylinder array with inclination, *Int. J. Heat Mass Trans*, *132*(2010), 7, pp, 071701, DOI No. 10.1115/1.4000061.

[18] Stanislaw L., *et al.*, Heat transfer coefficient in elliptical tube at the constant heat flux, *Thermal Science. 23*(2019), 4, pp: 1323-1332, DOI NO. 10.2298/TSCI19S4323L.

[19] Li, Z., *et al*., Numerical simulation of flow field and heat transfer of streamlined cylinders in cross flow, *J. Heat Transfer*, *128*(2006), 6, pp. 564-570.

[20] Razzaghi, H., *et al*., Numerical analysis of the effects of changeable transverse and longitudinal pitches and porous media inserts on heat transfer from an elliptic tube bundle, *J Theor App Mech-Pol*, *52*(2014), 3, pp. 767-780.

[21] Kong, Y. Q., *et al*., Air-side flow and heat transfer characteristics of flat and slotted finned tube bundles with various tube pitches, *Int. J. Heat Mass Trans*, *99*(2016), pp. 357-371.

[22] Mangrulkar, C. K., *et al*., Experimental and CFD prediction of heat transfer and friction factor characteristics in cross flow tube bank with integral splitter plate, *Int. J. Heat Mass Trans*, *104*(2017), pp. 964-978.

[23] Zhang, L., *et al.*, Numerical analysis of heat transfer enhancement and flow characteristics inside cross-combined ellipsoidal dimple tubes, *Case Studies in Thermal Engineering*, *25*(2021), pp. 100937.

[24] Hassan, M, A., *et al*., Hydrothermal characteristics of turbulent flow in a tube with solid and perforated conical rings. *International Communications in Heat and Mass Transfer*, *134*(2022), pp 106000.

[25] Kaood, A., Hassan, M, A., Thermo-hydraulic performance of nanofluids flow in various internally corrugated tubes. *Chemical Engineering and Processing - Process Intensification*, *154*(2020), pp. 108043.

[26] Gnielinski, V., New equations for heat and mass transfer in turbulent pipe and channel flow Int. *Chem. Eng*, *16*(1976), pp. 359-368.

[27] B. Petukhov, Heat transfer and friction in turbulent pipe flow with variable physical properties, *Advances in Heat Transfer*, *6*(1970), pp. 503-564.

RECEIVED DATE: 22.4.2023
DATE OF CORRECTED PAPER: 12.7.2023.
DATE OF ACCEPTED PAPER: 5.10.2023.